SAR ANALYSIS OF SPINAL MODULATION IMPLANTABLE DEVICE
Model MN0200
FCC ID: Y8L-MN0200

October 21, 2011

Submitted to:

Jim Judkins
Spinal Modulation
1135 O'Brien Dr.
Menlo Park, CA 94025

Submitted by:

Ian Wood and David Johns
CST of America
492 Old Connecticut Path, Suite 505
Framingham, MA 01701

SAR ANALYSIS OF SPINAL MODULATION IMPLANTABLE DEVICE
Model MN0200

October 21, 2011

Signed by:

Ian Wood
Application Engineer
CST of America
492 Old Connecticut Path, Suite 505
Framingham, MA 01701

Signed by:

David Johns
VP of Engineering and Support
CST of America
492 Old Connecticut Path, Suite 505
Framingham, MA 01701

1 Introduction

The Spinal Modulation MN0200 Implantable Neurostimulator is designed for patient pain relief by electrical stimulation of nerve bundles located in the spinal area. It communicates to an external Programmer thru a RF link using the MICS/MedRadio standard at 403 MHz. The RF communication is used initially by the clinician to program stimulation during implant and again during routine visits by the patient. The patient has their own Programmer that can be used to adjust stimulation levels daily. The radio antenna is located at the top of the implant device, referred to as the 'header', along with the stimulation lead ports and encapsulated in a clear plastic epoxy. The antenna is a wire coil in a cuboid shape with an approximate volume of 1 cubic centimeter. The electronics are housed inside a sealed titanium can. The entire assembly is implanted away from the spinal area in a location determined by the physician and typically near the iliac crest. The stimulation leads are routed from the header lead ports to the specific spinal nerve bundles.

A photograph of the implanted device, alongside the model used for simulation is shown below in Figure 1.

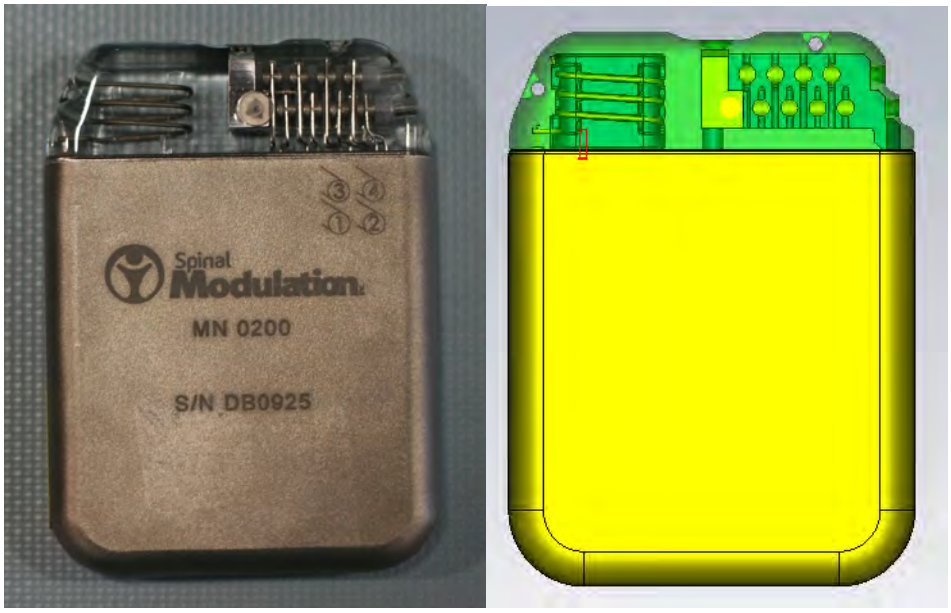

Figure 1: Image of physical device and imported model for simulation

The requirements for use of this band of frequencies are described in 47 CFR Part 95 [1]. In part 95.603(f) there is a requirement for certification. Part of that process includes the evaluation of the specific absorption rate (SAR) of body tissue exposed to the radiation from the implant. The limits for this device are described in 47 CFR Part 1 in section 1.1307 and in 47 CFR Part 2, Section 2.1093 [2]. The usage of the equipment is uncontrolled and therefore the limits are for a Partial Body value of 1.6 W/kg averaged over any 1 g of tissue volume and in the shape of a cube. The Whole Body limit for average SAR is at 0.08 W/kg.

The numerical method used to determine the SAR values is time domain simulation based on The Finite Integration Technique (FIT) [3-6]. FIT can be considered an extension of the Finite Difference time Domain (FDTD) technique as mentioned in the draft IEEE P1528.1 standard [7]. Details on the FIT method relevant to SAR calculation are provided in Appendix 1.

2 Scope

The purpose of this report is to show compliance of the Spinal Modulation implanted device SMI Model # MN0200, FCC ID# Y8L-MN0200, with 47 CFR Part 1 section 1.1307 and 47 CFR Part 2 section 2.1093 SAR values using the FIT calculation technique.

3 Results

The maximum computed SAR levels are below the limits as specified in 47 CFR Part 1, section 1.1307 and in 47 CRF Part2, section 2.1093.

Whole Body average SAR at 403 MHz	0.1585 mW/Body Weight (80 kg) = 0.001981mW/kg
dB below 0.08 W/kg limit	46.06 dB
Maximum 1g SAR at 403 MHz	10.32 mW/kg
dB below 1.6 W/kg limit	21.90 dB

4 Calculation Technique

The CST Microwave Studio simulation program was used. Microwave Studio uses the Finite Integration Technique (FIT) which in the time domain can be considered an extension of the FDTD method [3]. Details about FIT are provided in Appendix 1. FIT has been validated through numerous publications, for example Reference 6. **Examples of validation specific to SAR analysis include References 8 and 9**. Additionally, a series of benchmarks from the current draft of IEEE Std. 1528.1 were also conducted to show the validity of FIT for SAR calculations, and can be found in Appendix 2-6.

A SuperMicro workstation with 2Quad Core X5550 2.53 Ghz processors and 72 GB RAM was used during the simulations. Portions of the field analysis were run on an nVIDIA S1070 GPU for acceleration. The operating system used was Microsoft Windows Server 2008 R2, standard x64 Edition Service Pack 2. During computation 26,946,432 mesh cells were used which gave a solver memory requirement of 14,273 MB. The total simulation took 2 hours 5 minutes with 8 threads parallelized.

The simulation halted when the energy dropped to -60dB below the peak (Figure 2). At this level, truncation error introduced by terminating the transient signals is negligible, as shown by the absence of any ringing artifacts in the resulting frequency domain results. As such, results obtained through the transient simulation accurately reflect the steady state behavior of the device.

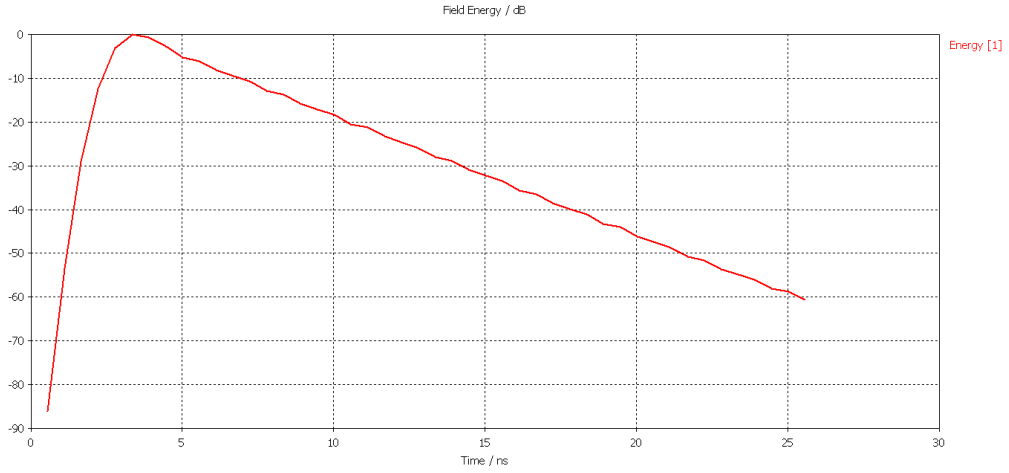

Figure 2: Energy decay plot. The Y axis units are dB with 0dB set as a reference at the peak energy.

4.1 Volume of Simulation

A CAD model supplied by Spinal Modulation of the implant device model MN0200 was imported into CST Microwave Studio. The model was healed and combined with the Visible Human Project's HUGO voxel model of the human body. The HUGO model is commonly used in the industry for the purpose of SAR analysis of implantable devices at these frequencies. Material properties were assigned to the model as described in the table below; biological materials were defined using HUGO data at 450 MHz [10]. The total volume of human body model considered for the analysis was 594 X 341 X 866 mm^3, extending roughly from the knees to the shoulders with 1mm^3 resolution. An additional 125 mm of vacuum, beyond the extents of the body model, was also included to ensure the model was sufficiently isolated from the simulation volume boundaries. The space was terminated in a Perfectly Matched Layer (PML) absorbing boundary condition.

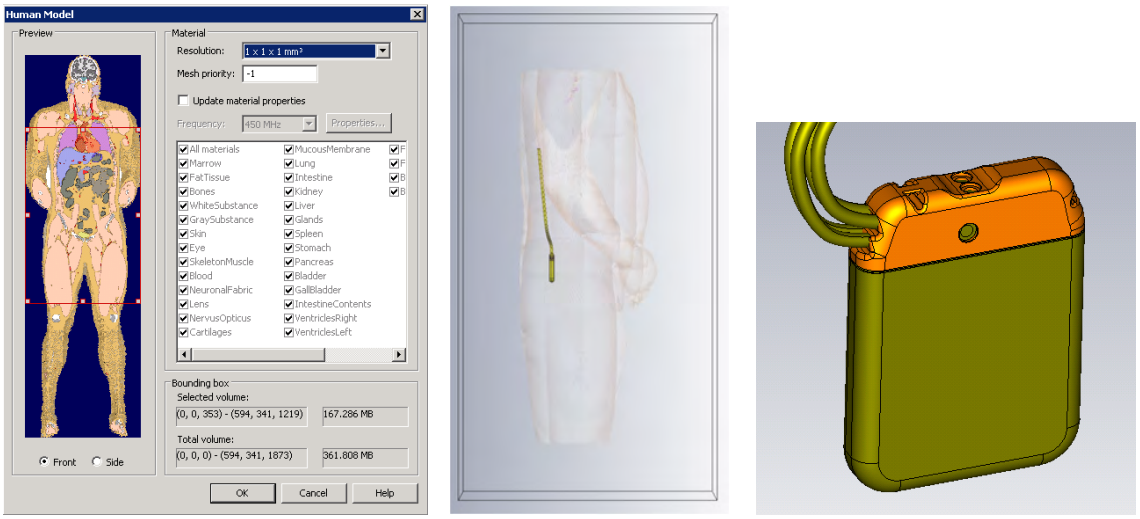

Figure 3: CAD and biological models imported into simulation software

Material properties at 403MHz

Parts	*Material name*	*Material type*	*Permittivity*	*Loss tangent (at 403MHz)*	*Conductivity*
Metal case / Leads	*Titanium*	*Lossy Metal*	-	-	*2.38e7 S/m*
Antenna housing	*Epotek 301*	*Dielectric*	*4*	*0.016*	-
Antenna Core	*Acrylic*	*Dielectric*	*3*	-	-
Antenna Wire	*Titanium*	*Lossy Metal*	-	-	*2.38e7 S/m*

Tables below list the dielectric properties used in the HUGO voxel model implant area for SAR simulation. HUGO model differences in dielectric and conductivity properties are less than 5% between 450 and 403 MHz shown with selected values in tables below. This discrepancy is far smaller than the 21.90 dB margin by which the device exceeds specification, noted in Section 3.

Table of dielectric and conductivity property values compare 403 and 450 MHz are within 5%.

Four term Cole-Cole expression for human tissues							
based on data compiled by Camelia Gabriel for Brooks Air Force Base (Tech. Report AL/OE-TR-1996-0037)							
valid from 10 Hz to 100 GHz.	http://www.fcc.gov/oet/rfsafety/dielectric.html						
403 MHz TISSUE	blood	bone cancellous	fat (not infiltrated)	muscle	nerve (spinal cord)	skin - dry	skin-wet
εr'	**64.2**	**22.4**	**5.6**	**57.1**	**35.4**	**46.7**	**49.8**
σ (S/m)	**1.351**	**0.235**	**0.041**	**0.797**	**0.447**	**0.689**	**0.670**
450 MHz TISSUE	blood	bone cancellous	fat (not infiltrated)	muscle	nerve (spinal cord)	skin - dry	skin-wet
εr'	**63.7**	**22.2**	**5.6**	**56.8**	**34.9**	**45.8**	**49.2**
σ (S/m)	**1.367**	**0.244**	**0.042**	**0.809**	**0.460**	**0.709**	**0.687**

Table of % delta dielectric and conductivity properties compare 403 and 450 MHz are within 5%.

	blood	bone cancellous	fat (not infiltrated)	muscle	nerve (spinal cord)	skin - dry	skin-wet
450/403 MHz %delta er'	0.7	1.1	0.3	0.6	1.4	2.1	1.3
450/403 MHz %delta (S/m)	-1.2	-3.8	-1.9	-1.5	-2.8	-2.8	-2.5

4.2 Density of Mesh

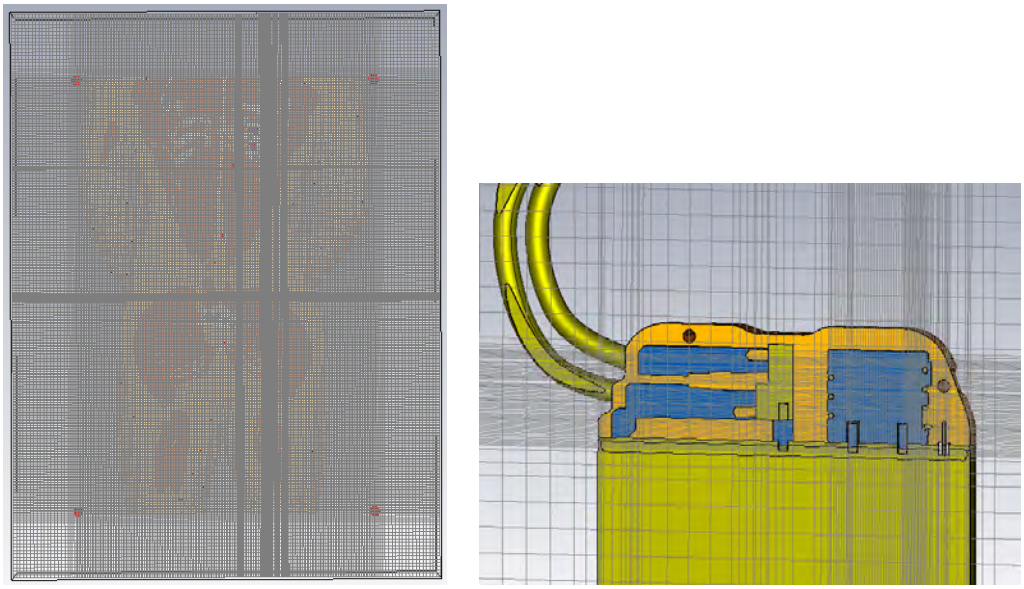

Figure 4: Mesh volume and density around implant

The maximum allowable cell size used in this model's mesh is 1/20th of a free space wavelength at 0.6 GHz, or 25mm. The actual largest mesh cell utilization, because of the uniform volume mesh was substantially smaller than allowed, was 6.8 mm. The smallest cell size in the mesh is 0.15 mm, less than half the 0.3175 mm radius of the helix antenna wire. The mesh automatically adapts to ensure that there are at least 20 cells per wavelength inside any dielectric materials where the wavelength is smaller. The time-step was 3.508511e-004 ns and 72,910 time-steps were computed. A Gaussian pulse was used for the excitation with a bandwidth from 0 to 600 MHz.

The antenna wire was modeled as a circular cross-section, with a minimum of 2 to 4 mesh cells in the antenna cross-section. The Perfect Boundary Approximation (PBA) technique [6] increases accuracy of modeling the curved wire. The radius of the wire was 0.3175 mm and the mesh cells on the cross-section were 0.15 mm per side.

5 Device Simulated

5.1 Mechanical Characteristics

CAD models of essential parts of the implanted device were imported to the simulator in order to enable a correct representation of the antenna function. As such the model used in simulation is a prototype of the actual device.
The essential features necessary for SAR modeling:

- Antenna wire
- Plastic antenna core
- Stimulation lead ports
- Stimulation leads
- Epoxy header encapsulation
- Internal antenna matching circuit

The implant device was given priority over the voxel tissue using a mesh priority hierarchy. The device was aligned and rotated to correspond with the approximate installed location, as shown in Figure 3 and 5.

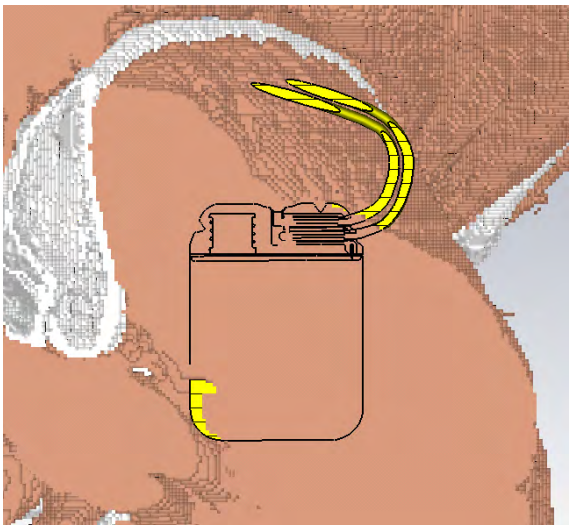

Figure 5: Implant device inserted into tissue

For the particular test device model, the features that were considered essential included the orientation of the device, the device dimensions and location of the antenna, modeling of metal or other conducting components, and free space around the HUGO model.

The device leads were generated within CST MWS, using a circular cross section substantially larger wire radius (2.8448 mm) than is present in reality (0.1524 mm). This approach was less expensive for computation. The increased radius presents a worst case for coupling to the device, since the larger electrical size increases the exposure area to the device antenna. The device leads extend outward from the opposite side of the device from the antenna, so induced currents should be minimal. Potential resonances on the leads will also be strongly suppressed by the high material losses in the body tissue. .The observed simulated power loss density in proximity of the leads was negligible, as shown in Section 7.

Port 1 was connected to the cross section of the coaxial feed of the helix antenna operating at 403 MHz. The 402 to 405 MHz MICS/MedRadio band has 3 MHz bandwidth; < 1% bandwidth. The 403 MHz center frequency was chosen to be representative of the SAR.

5.2 Electrical Characteristics of Simulation

The input power excited into the antenna feed in the simulation was – 8dBm or 0.1585 mW peak, which corresponds to maximum possible values for the physical device.

The SAR calculations are based on a continuous sinusoid (CW) at 403 MHz. In reality, the antenna will operate over a narrow band associated with data. The implanted RF system operates by responding to a communication session initiated by an external control unit being done in a half duplex manner. There are periods of time in which no transmission takes place from the implanted device to the control unit during a session. During that time the implanted device is in the receive mode and is not transmitting. When not within a communication session the implanted device is also not transmitting. The maximum expected RF communication session per day is 8 minutes to conserve battery life of the implant. The resulting reduction of duty cycle from CW makes the SAR calculation very conservative in that the SAR power levels have been calculated for CW values at peak operation.

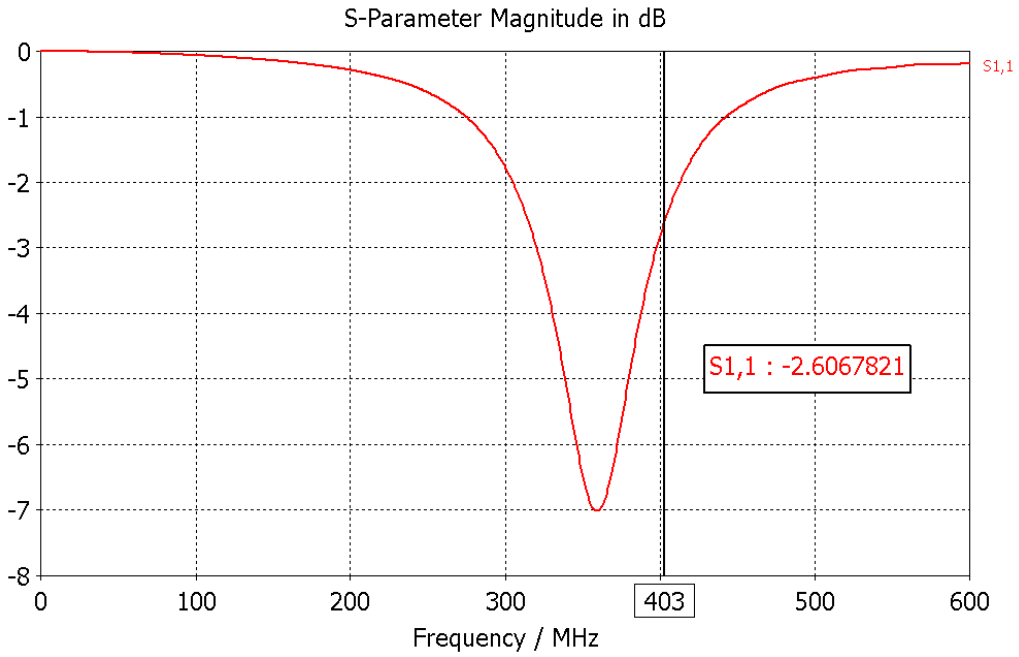

Figure 6: S parameters with waveguide port, without matching circuit

Figures 7 shows the matching circuit used in the device and included in simulation, as well as the resulting s11 parameter.

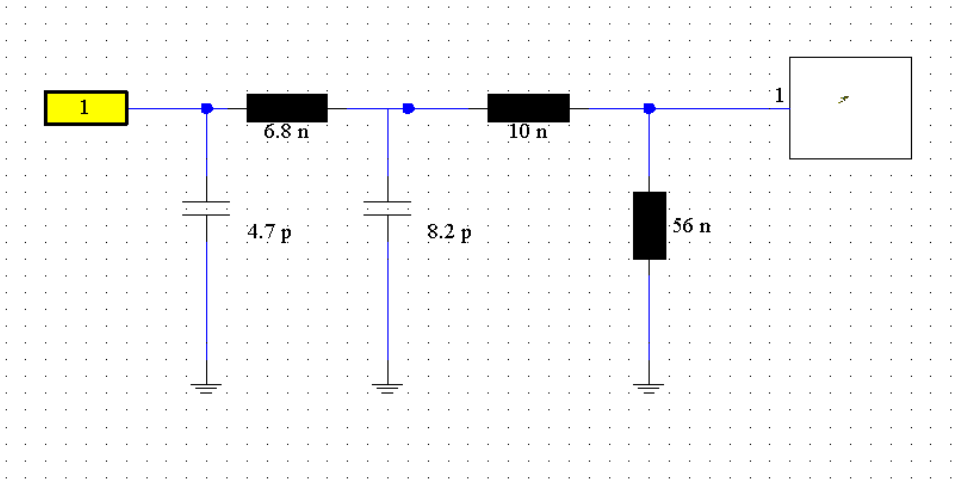

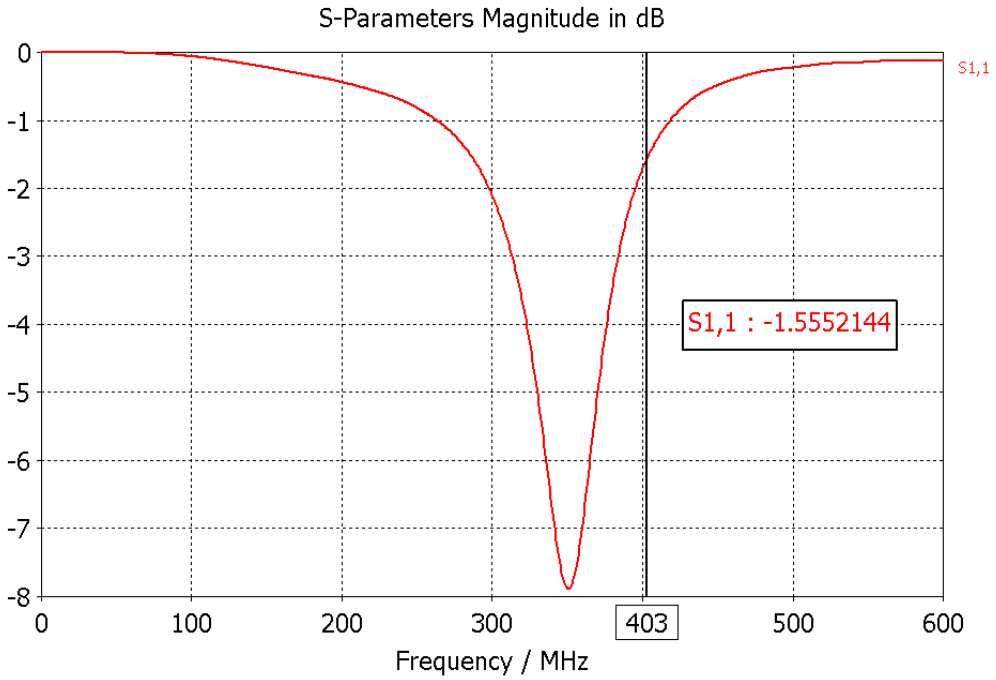

Figure 7: Antenna Matching Circuit and S parameters

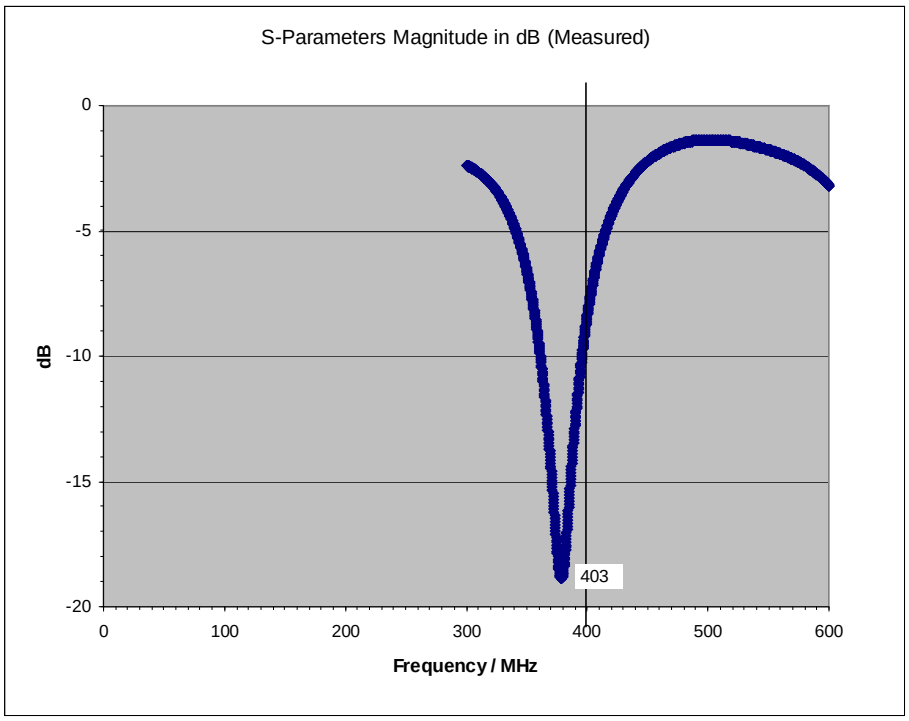

Figure 8: Measured S parameters of Device

Figures 7 and 8 compare the s parameter results of the simulated model (including the matching circuit used in the physical device) and the measured results of the fabricated device. The resonant frequency is consistent, however the magnitude of reflection is higher in the simulated results. This discrepancy is likely due to the difference in surround material between the two cases. While the simulated results are defined within the inhomogeneous HUGO material dataset with several different tissue types in close proximity to the antenna, while the measurement was conducted in a homogeneous block of tissue stimulant.

Materials in close proximity to the device antenna can influence its effective impedance. The implantation procedure, and variation in patient body structures, inherently results in an amount of uncertainty in the installed location. To remove this uncertainty, a second matching circuit designed for optimal matching in the exact simulated case was also designed and analyzed. This circuit and the resulting s11 plot are shown below in Figure 9.

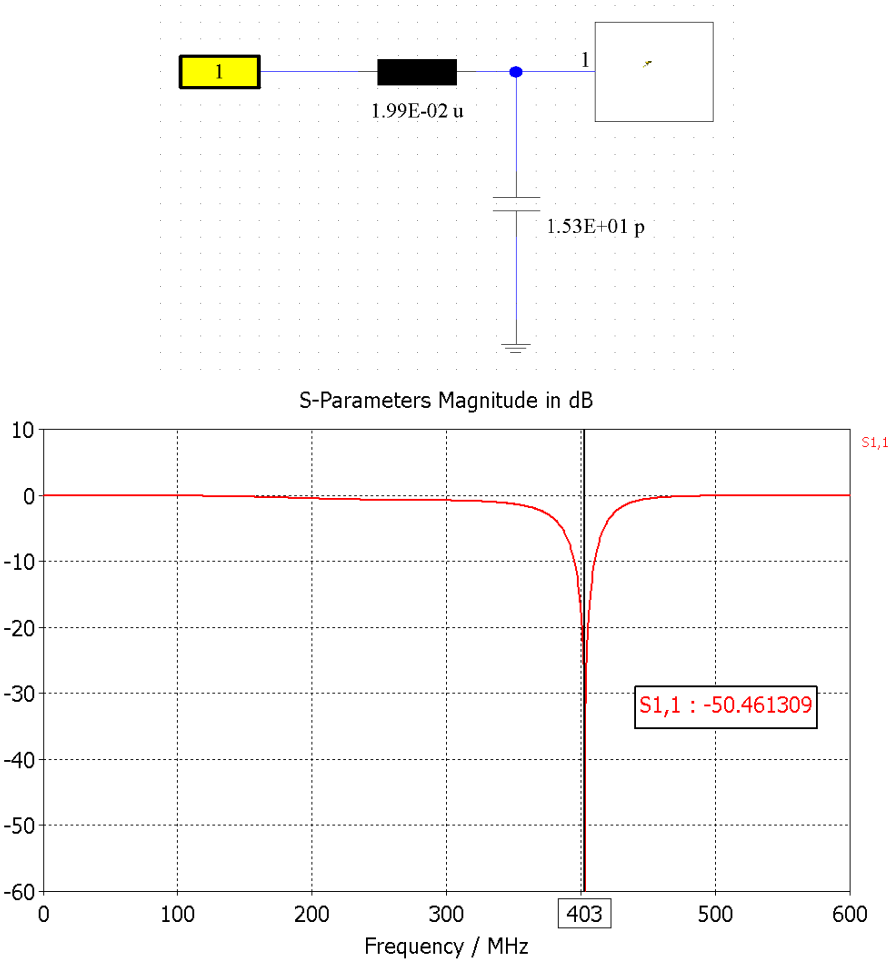

Figure 9: Custom Matching Circuit and S parameters

The custom circuit uses a lumped inductor and capacitor to match the antenna impedance at 403 MHz. The S11 is below -50dB indicating that over 99% power is delivered to the antenna. This is considered to be the worst case situation since the maximum power of -8 dBm is delivered to the antenna. As such, this circuit was used as the basis for subsequent SAR results.

6.0 Calculation of SAR

The implanted device is modeled at 403 MHz. The SAR calculation can be carried out as a post-processing step after the simulation. The power loss density is monitored throughout the tissue and used to calculate the SAR values and fields. The Specific Absorption Rate (SAR) is defined as the time derivative of the incremental energy (dW) absorbed by (dissipated in) an incremental mass (dm) contained in a volume element (dV) of a given mass density (ρ):

$$SAR = \frac{d}{dt}\left(\frac{dW}{dm}\right) = \frac{d}{dt}\left(\frac{dW}{\rho \cdot dV}\right)$$

The SAR value is expressed in units of watts per kilogram (W/kg).

1g averaged SAR: SAR is given as a numerical value per volume element and becomes a space distribution function. For this function, the mass mean value in an arbitrary tissue volume is called the local SAR. Typical local SAR values are averaged in tissue masses of 1g as specified by **IEEE P1528.1** [7].

IEEE P1528.1 is an averaging method according to the current standard draft "IEEE P1528.1™/D1.00 Draft Recommended Practice for Determining the Peak Spatial-Average Specific Absorption Rate (SAR) in the Human Body from Wireless Communications Devices, 30 MHz - 6 GHz: General Requirements for using the Finite Difference Time Domain (FDTD) Method for SAR Calculations". Compared to the IEEE C95.3 method it uses an additional criterion that limits the air volume in valid averaging cubes to 10%.

Whole-body-averaged SAR: The value is obtained by dividing the total power absorbed in the human body by the full body weight. It is also possible to define a sub volume by picking objects or by defining extents.

Density of muscle tissue is 1.06 kg/liter or 1.06 gm/cm³. There approximately 1,000 mm³ per cubic centimeter, or 1000 voxel simulation cells per cubic centimeter for 1 gram of muscle tissue.

7.0 Power Loss Calculations

Figure 10 shows the distribution of SAR projected on the full 3D model. The maximum SAR occurs internally, nearby to the implant device and the value is 0.01032 W/kg with - 8dBm excited power.

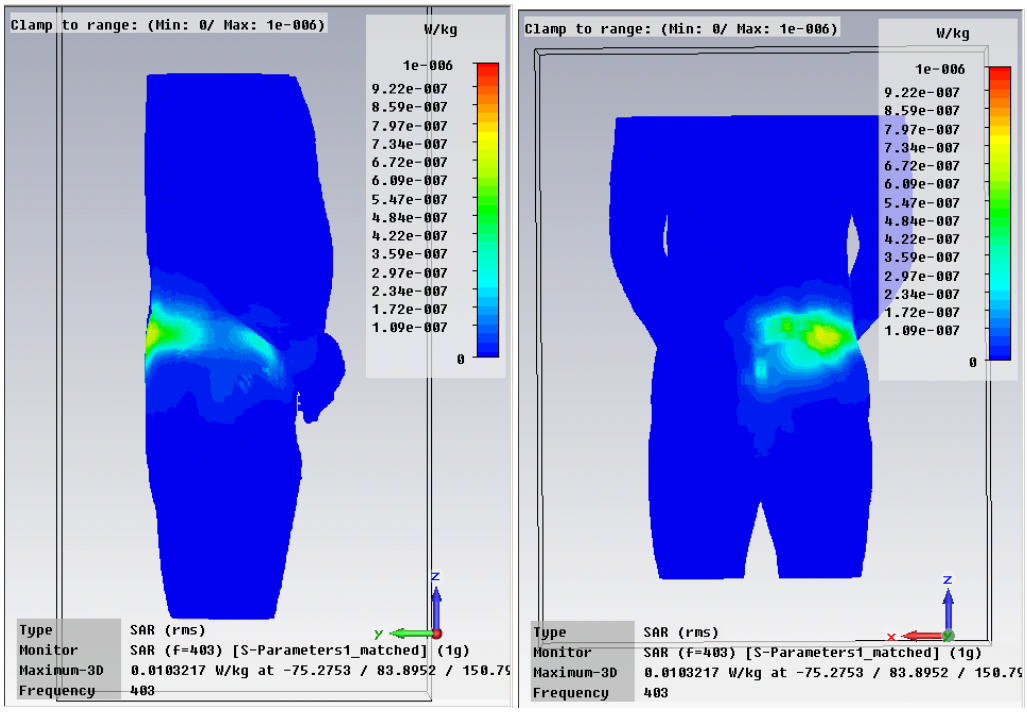

Figure 10 SAR distribution on 3D model

Figure 11 shows the distribution of SAR projected on several 2D cut-planes in the model, aligned to show the maximum SAR location near the implant antenna.

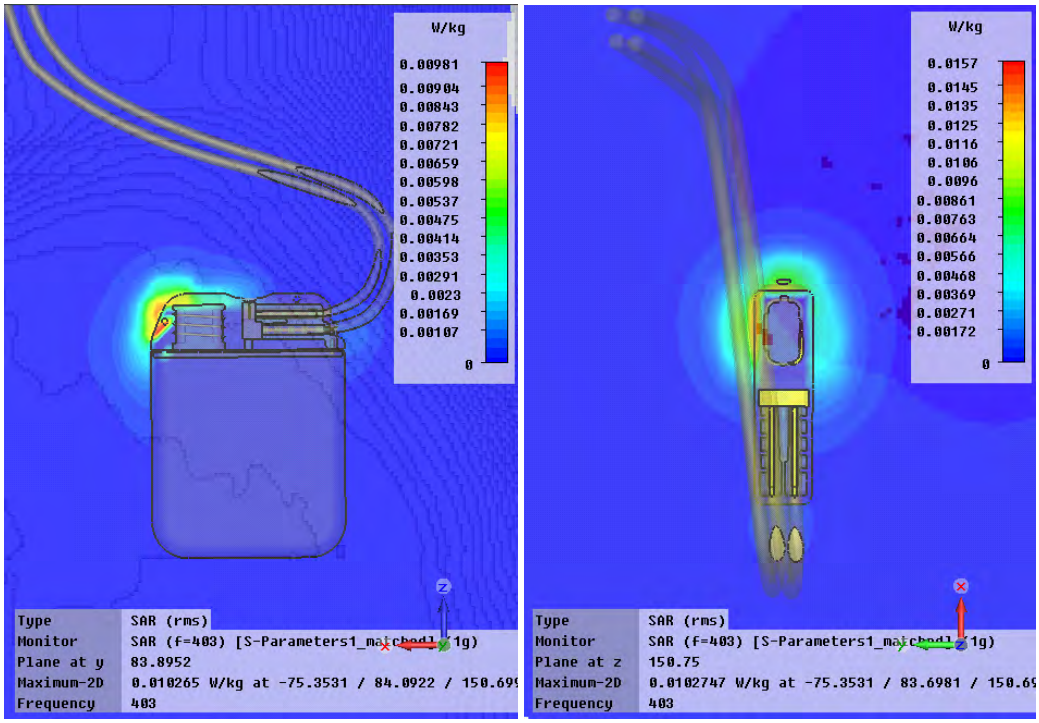

Figure 11: SAR distribution on 2D cut planes

8.0 Conclusions

The simulated SAR values are well below the limits described in 47 CFR Part 1 in section 1.1307 and in 47 CFR Part 2, Section 2.1093 [2].

- Maximum 1g averaged SAR is 10.32 mW/kg, well below the limit of 1.6 W/kg
- Maximum whole body SAR is 0.001981mW/kg, well below the limit of 0.08 W/kg

We have reduced uncertainty in the simulation results by considering the worst-case power level and assuming all power is delivered to the antenna. There is a large margin between the predicted SAR values and the SAR limit levels. Errors associated with the numerical model are expected to be well within this margin. The mesh density was very fine (at least 20 cells per wavelength in the dielectric material), so dispersion errors were minimized. The simulation ran until the total energy decayed by 60dB, so the field values had fully converged. A recent international inter-laboratory study concluded that the agreement in calculated SAR between participating laboratories was very similar to the agreement obtained in inter-laboratory comparisons involving SAR measurements [13]. CST's Microwave Studio was one of four FD-TD type tools used in the study.

9.0 References

[1] 47 CFR Part 95

[2] 47 CFR Part 1; 47 CRF Part 2

[3] S. Gutschling, H. Krüger, T. Weiland: Modelling Dispersive Media Using the Finite Integration Technique. Proceedings of the 14th Annual Review of Progress in Applied Computational Electromagnetics (ACES 1998), Vol. 2, March 1998, pp. 832-837

[4] Weiland, T.: A discretization method for the solution of Maxwell's equations for six-component fields: Electronics and Communication, (AEÜ), Vol. 31, pp. 116-120, 1977.

[5] Weiland, T.: Time domain electromagnetic field computation with finite difference methods. International Journal of Numerical Modelling, Vol. 9, pp. 295-319, 1996.

[6] Krietenstein, B.; Schuhmann, R.; Thoma, P.; Weiland, T.: The Perfect Boundary Approximation technique facing the challenge of high precision field computation: Proc. of the XIX International Linear Accelerator Conference (LINAC'98), Chicago, USA, pp. 860-862, 1998.

[7] IEEE P1528.1/D1.00 IEEE Draft Recommended Practice for Determining the Peak Spatial-Average Specific Absorption rate (SAR) in the Human Body from Wireless Communication Devices, 30 MHz – 6 GHz: General requirements for using the Finite Difference time Domain (FDTD) Method for SAR Calculations

[8] O. Sotoudeh & T. Wittig: Electromagnetic Simulation of Mobile Phone Antenna Performance, Microwave Journal, January 2008.

[9] Rugged Printable Dipole Reference for SAR and Free Space Measurement Verifications: Michael Kanda, Giorgi Bit-Babik, Miguel Richard, and C-K. Chou. IEEE MTT-S International Microwave Symposium, Seattle, WA. June 2-7, 2002.

[10] Tissue dielectric parameters are based on http://www.nlm.nih.gov/research/visible/visible_human.html

[11] ANSI/IEEE C95.1-1992 IEEE Standard for Safety Levels with Respect to Human Exposure to Radio Frequency Electromagnetic Fields, 3 kHz to 300 GHz

[12] IEEE Std C95.3-2002 IEEE Recommended Practice for Measurements and Computations of Radio Frequency Electromagnetic Fields With Respect to Human Exposure to Such Fields, 100 kHz–300 GHz

[13] An International Inter-laboratory Comparison of Mobile Phone SAR Calculation with CAD-based Models: Martin Siegbahn1*, Giorgi Bit-Babik2, Jafar Keshvari3, Andreas Christ4, Benoît Derat5, Vikass Monebhurrun6, Christopher Penney7, Tilmann Wittig8.

1. Ericsson AB, Sweden. 2. Motorola Inc, USA. 3. Nokia Corporation, Finland. 4. IT'IS foundation, Switzerland. 5. Sagem Mobiles, France. 6. Supelec, France. 7. Remcom Inc, USA. 8. CST AG, Germany.

[14] IEEE Std. 1528-2003, IEEE Recommended Practice for Determining the Peak Spatial-Average Specific Absorption Rate (SAR) in the Human Head from Wireless Communications Devices: Measurement Techniques

Appendix 1: Finite Integration Technique (FIT)

The SAR simulations performed by CST are based on the Finite Integration Technique (FIT) [5].

The Finite Integration Technique (FIT) in time domain can be regarded as an extension of FDTD [7] in the following context:

a) The electric field components are spatially located on the edges of a Cartesian coordinate system structured mesh composed of rectangular cells (hexahedral mesh)
b) The magnetic field components are spatially located on the edges of a Cartesian coordinate system structured mesh composed of rectangular cells (hexahedral mesh) which is offset from the electric field mesh by ½ mesh cell in each direction
c) The solution method uses a finite-integral approximation to Maxwell's curl equations, rendering them discrete in space and time in the form of the so called Maxwell Grid equations. The method is inherently second order accurate and can include non-uniform meshes.
d) The solution of the Maxwell Grid equations for the electric and magnetic fields is performed using a fully explicit leapfrog time stepping process.
e) Gauss's laws are implicitly enforced, the fields are divergence-free, and charge is conserved.
f) The time-stepping algorithm is non-dissipative in that there is no spurious decay of energy due to non-physical artifacts of the algorithm and artificial dissipation is not required for stability.

The FIT method used in CST's Microwave Studio™ can be considered an enhanced form of FDTD. A Perfect Boundary Approximation (PBA) is used to increase the accuracy of the modeling of curved boundaries. This is described in reference [6] and examples of the improved accuracy are provided for several applications.

Appendix 2 Free Space Characteristics

As a validation case for SAR results obtained using the Finite Integration Technique (FIT), the free space dispersion characteristics benchmark contained with [7] was simulated.

As specified in [7] a 120 mm wide waveguide structure was excited with a series of TE and TM modes with different dielectric loads. A set of electric field probes were aligned and placed according to the benchmark specification, and the wave numbers were derived from the resulting signals and compared with theoretical values to gauge the accuracy of the FIT code.

Figure 2-1 shows the TE mode field distribution generated in CST, compared with the analytical distribution described in [7]. The two track closely, and only a minimum error (plotted in blue) is present.

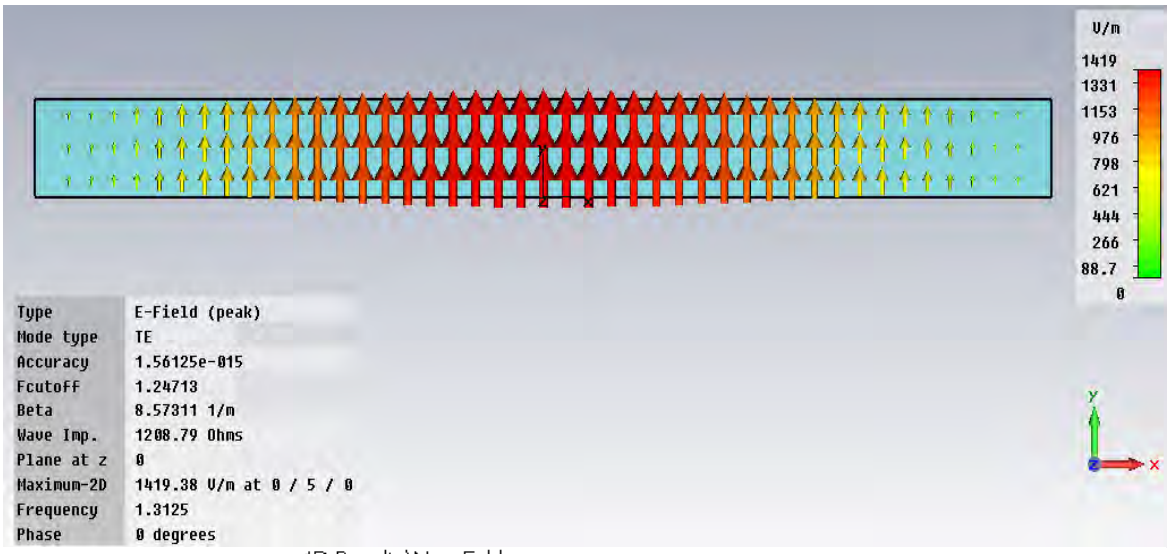

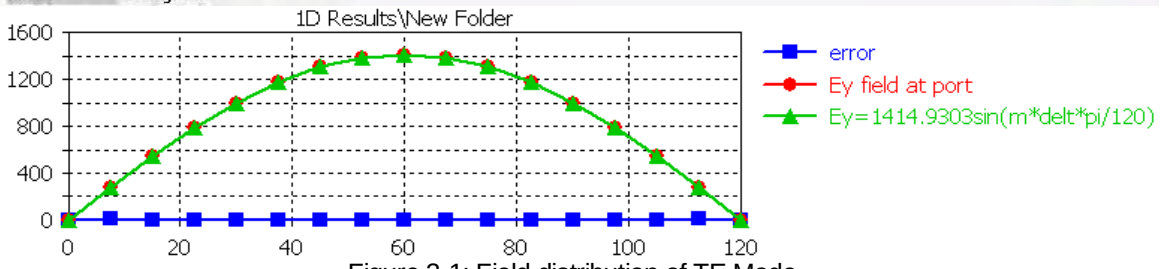

Figure 2-1: Field distribution of TE Mode

Similarly the TM mode field distribution is shown below in Figure 2-2 and compared with the analytical form presented in [7]; error is again minimal.

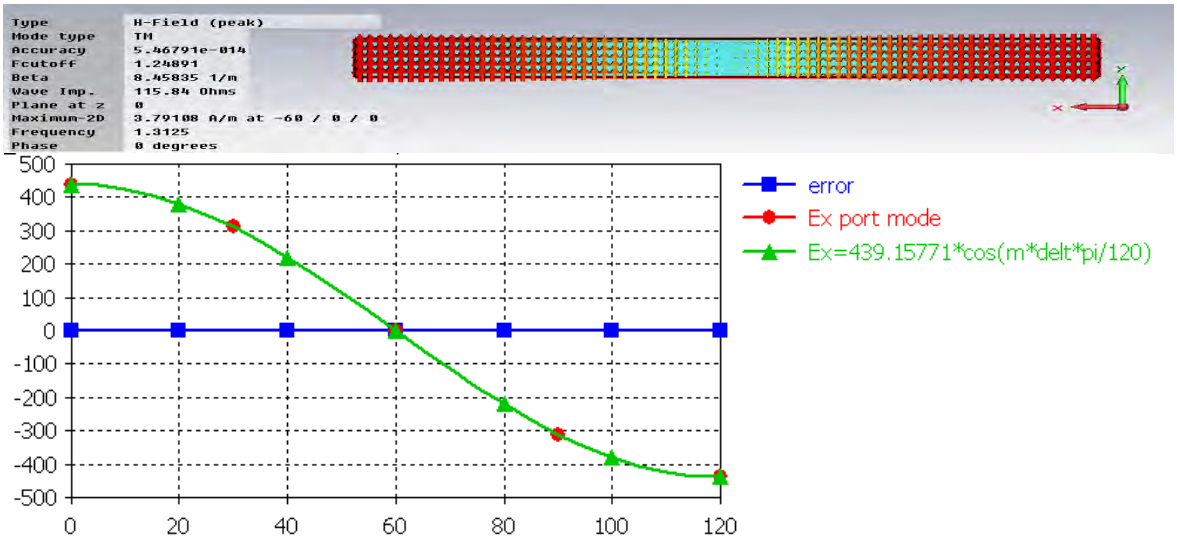

Figure 2-2: Field Distribution of TM Mode

For each mode and material combination, wave numbers were derived on both a homogeneous and inhomogeneous grid. For the homogeneous case, a cell size of 10 mm, as specified in [7] was utilized. The inhomogeneous grid was generated based on the step ranges provided in [7]. Both mesh grids are shown below in Figure 2-3.

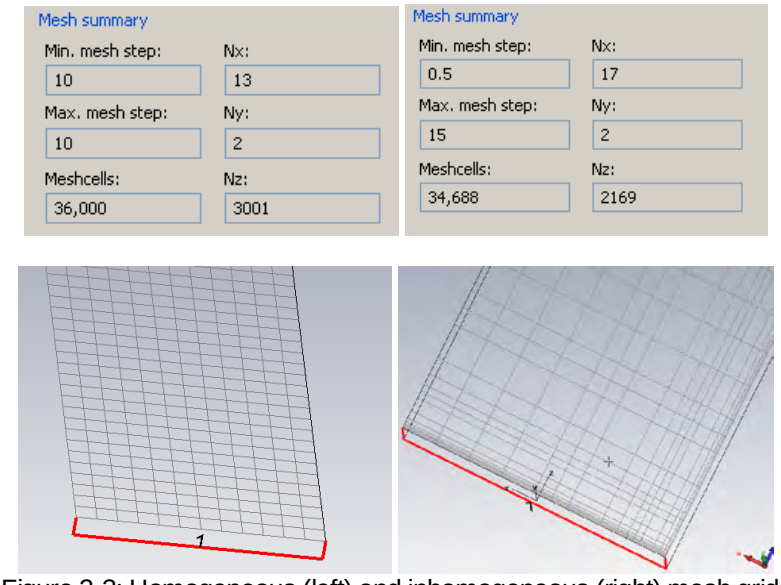

Figure 2-3: Homogeneous (left) and inhomogeneous (right) mesh grids

The Gaussian pulse described in [7] was generated and used as the excitation for each simulation case. It is plotted below in Figure 2-4.

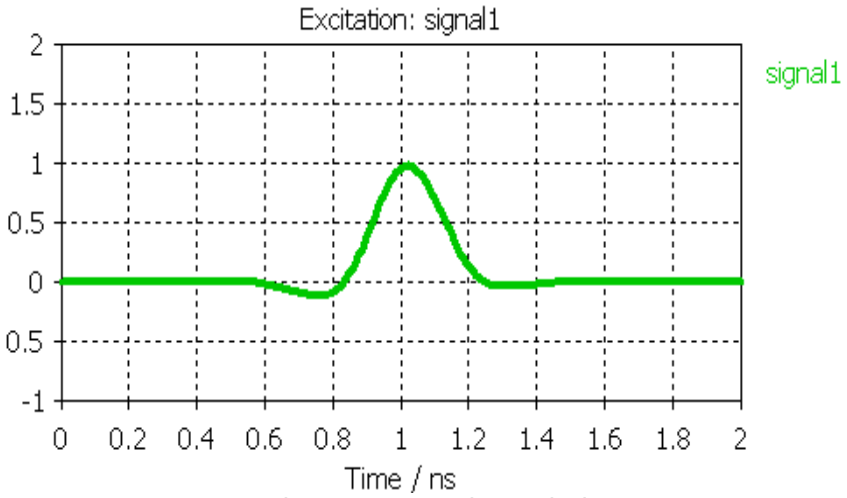

Figure 2-4: Gaussian excitation

The simulation was run for duration of 100 ns for the TE modes; for several of the TM modes the energy near cutoff took longer to decay, and the simulation time was increased to several thousand ns in order to satisfy the ripple criteria stipulated in [7]. The wave numbers were derived based on the probe signals according to the formulas listed in [7] and are plotted in Figure 2-5. The peak percentage error in frequency ranges from 5% above cutoff was then calculated and reported below in Table 2-1.

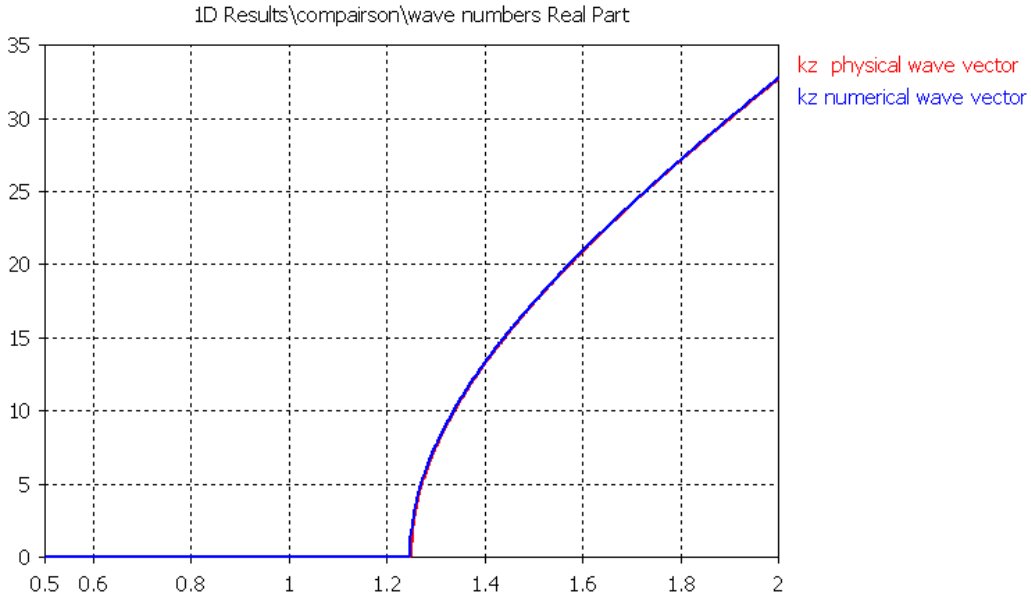

Figure 2-5: Example simulated wave number compared with analytical (physical) result

	Limit for code compliance	TE			TM		
ε_r		1	2	2	1	2	2
σ [S/m]		0	0	0.2	0	0	0.2
numerical f_{cutoff} [MHz]		1247	882	<500	1247	882	<500
max. dev. of simulated Re$\{k_z\}$ from numerical reference [%][4] homogeneous grid	±2%	1.79%	1.73%	0.556%	0.85%	2.458%	0.558%
max. dev. of simulated Im$\{k_z\}$ from numerical reference [%] homogeneous grid	±2%	n. a.	n. a.	2.7%	n. a.	n. a.	2.7%
max. dev. of simulated Re$\{k_x\}$ from numerical reference [%] homogeneous grid	±2%	9.3e-6%	7.1e-6%	2.8e-4%	1.27e-5%	8.79e-5%	5.36e-5%
max. dev. of simulated Re$\{k_z\}$ from numerical reference [%] inhomogeneous grid	±10%	3.2%	3.2%	1.15%	4.28%	4.80%	1.47%
max. dev. of simulated Im$\{k_z\}$ from numerical reference [%] inhomogeneous grid	±10%	n. a.	n. a.	10.15%	n. a.	n. a.	10.14%
max. dev. of simulated Re$\{k_x\}$ from numerical reference [%] inhomogeneous grid	±10%	0.39%	0.392%	0.396%	0.394%	0.395%	0.394%

Table 2-1: Percentage error for simulated wave numbers

For several of the cases (indicated in red), the percentage error slightly exceeds the draft specification. While the extent to which it exceeds spec is minimal, it is worth noting that when the actual maximum mesh settings used in the device simulation (20 lines per wavelength) are tested, the relative error is reduced well below the specification. In Figure 2-6, the percentage error is plotted for a number of mesh step sizes. 20 lines per wavelength would correspond to a mesh step size of 5 mm and is well below the draft specification throughout.

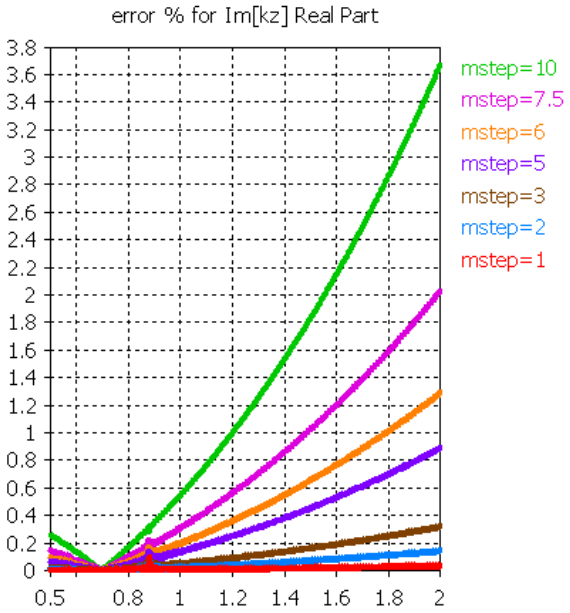

Figure 2-6: Percentage error of wave number for varied mesh density

Appendix 3 Planar Dielectric Boundary

As a validation case for SAR results obtained using the Finite Integration Technique (FIT), the reflection coefficient was derived from the simulated results of planar dielectric boundary as discussed in [7].

As specified in [7] a 120 mm wide waveguide structure was excited with a series of TE and TM modes. These modes were incident on a planar dielectric interface between the initial vacuum section and a second section with varied permittivity. The length of the vacuum section was greater than 120 mm as specified in [7]. Two sets of probes were used as defined in [7] to determine the wave number in the second media and the reflection coefficient in the first media. The configuration is shown below in Figure 3-1.

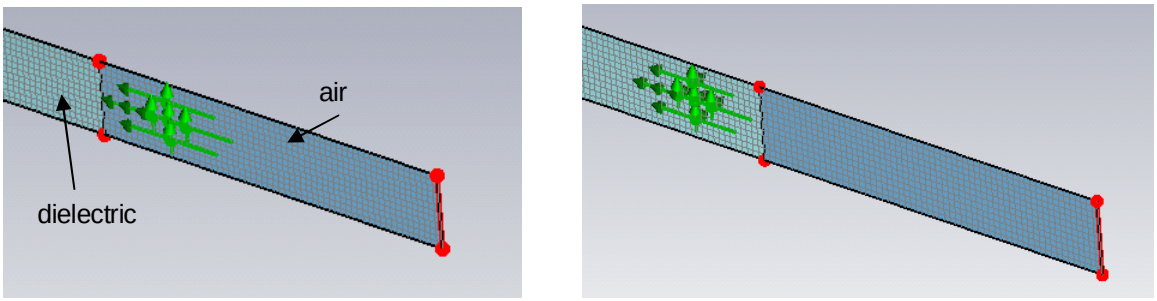

Figure 3-1: Probe configurations for the reflection coefficient (left) and the wave number (right)

As specified in [7] a uniform homogeneous mesh grid was utilized with a step size of 10 mm.
The resulting reflection coefficient and wave numbers were calculated and compared with the numerical (analytical) solution for a standard FDTD code. The resulting error percentages for the different mode and dielectric conductivity cases are listed below in Table 3-1.

	Limit for code compliance	TE		TM
ε_r		4	4	4
σ [S/m]		0	0.2	0
max. dev. of simulated Re$\{k_z\}$ from numerical reference [%] f>1.26GHz	5.0	2.6	2.21	2.68
max. dev. of simulated Im$\{k_z\}$ from numerical reference [%] f>1.26GHz	5.0	n. a.	8.48	n. a.
max. dev. of simulated Re$\{r\}$ from numerical reference [%] f>1.26GHz	5.0	1.68	1.78	***
max. dev. of simulated Im$\{r\}$ from numerical reference [%] f>1.26GHz	5.0	n. a.	35.5	n. a.

*****The extracted reflection coefficient has much better agreement with physical reference than the numerical reference. See Figure 3-3.**

Table 3-1: Percentage errors of simulated wave numbers and reflection coefficients

The error in the imaginary part of the propagation constant for the lossy material case is substantially higher (8.48%) than the specified error percentage limit (5%). The error can be reduced to below the specified level by using a finer mesh, as demonstrated in the previous Appendix 2.

Regarding the error in reflection coefficient, the absolute values for the simulated (FIT) imaginary part of the reflection coefficient and wave number are small. The standard requires that these values are normalized by the also small numerical reference (FDTD) values. This results in large error percentages for small differences in result values. The errors are small in absolute terms, but large in percentage terms. Additionally, the numerical results for comparison in [7] are based on an FDTD formulation rather than actual physical (analytical) results.

Below are the formulas for the FDTD based solutions of the reflection coefficient for the TE and TM modes simulated [7]:

$$r_{TE} = \frac{\sin k_{1z}\Delta s - \sin k_{2z}\Delta s}{\sin k_{1z}\Delta s + \sin k_{2z}\Delta s} \qquad r_{TM} = \frac{\varepsilon_1 \tan\frac{k_{2z}\Delta s}{2} - \varepsilon_2 \tan\frac{k_{1z}\Delta s}{2}}{\varepsilon_1 \tan\frac{k_{2z}\Delta s}{2} + \varepsilon_2 \tan\frac{k_{1z}\Delta s}{2}}$$

In the above formulas, the deltaS term indicates the mesh step size used and represents error introduced by the quantization. The actual physical formulas for the refleciton coefficients are presented below [7]:

$$r_{TE\_physical} = \frac{k_{1z} - k_{2z}}{k_{1z} + k_{2z}} \qquad r_{TM\_physical} = \frac{\varepsilon_1 k_{2z} - \varepsilon_2 k_{1z}}{\varepsilon_1 k_{2z} + \varepsilon_2 k_{1z}}$$

Below in Figure 3-2, the reflection coefficient from the FIT simulation, extracted from the probes, is plotted and compared with both the FDTD numerical solution and the physical (analytical) solution, for the case of the TE mode.

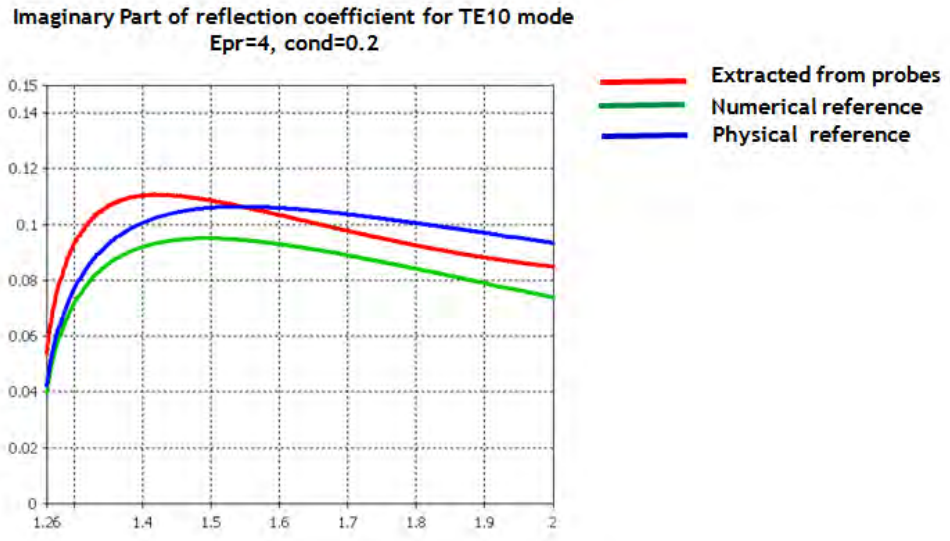

Figure 3-2: Comparison of simulated, numerical reference and physical (analytical) results for reflection coefficient of TE mode

It is clear that while the FIT simulation results differ from the numerical FDTD reference, they are comparable or provide better accuracy for much of the bandwidth compared with the actual physical (analytical) formulation of the reflection coefficient.

This tendency is even more dramatic in the case of the TM mode, shown below in Figure 3-3, where the numerical reference (FDTD) shows substantial deviation from the physical (analytical) formula, whereas the FIT (extracted from probes) simulated solution still has good accuracy.

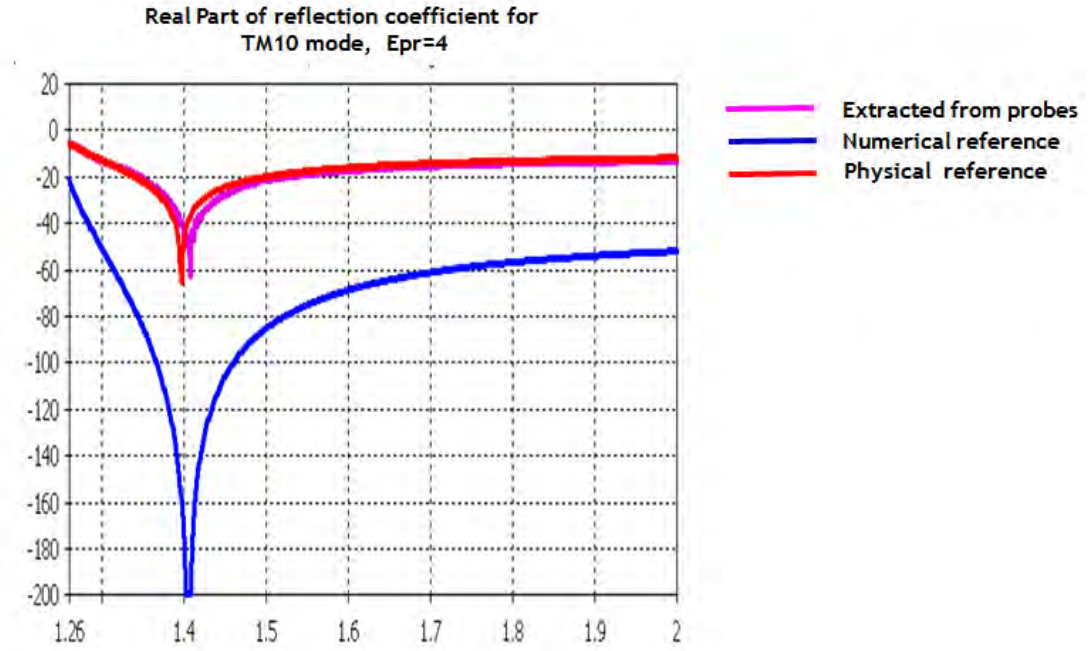

Figure 3-3: Comparison of simulated, physical and numerical references for reflection coefficient of TM mode

Appendix 4 PML Absorbing Boundary Conditions

As a validation case for the Perfectly Matched Layer (PML) absorbing boundary condition implementation used in CST Microwave Studio, the aligned absorbing boundary condition test described in [7] was run.

A 120mm rectangular section of vacuum filled waveguide was terminated in an absorbing boundary utilizing the PML open boundary within CST. As specified in [7] a homogeneous mesh step of 10 mm was used throughout the simulation volume. The excitation parameters described in [7] were utilized to generate both TE and TM excitation test cases and are listed below in Table 4-1. The simulation was run for 200 ns.

	TE	TM
ε_r	1	1
σ [S/m]	0	0
f_0 [MHz]	1200	1200
t_0 [ns]	1	1
τ [ns]	.2	.2
simulated time [ns]	200	200
waveguide length [m]	0.120	0.120
remaining signal ripple [%]	0.038	0.15

Table 4-1: Simulation Parameters

The resulting simulation geometry, along with the mesh and probe locations used to derive the reflection parameter as described in [7] are shown below in Figure 4-1.

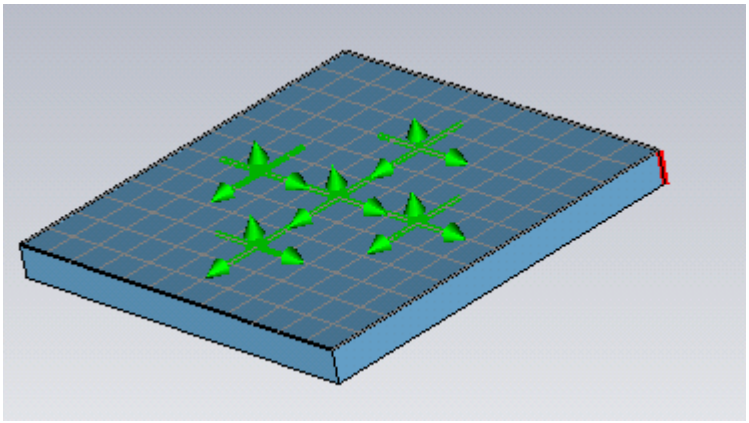

Figure 4-1: ABC benchmark model geometry with mesh and probes visible.

The resulting reflection coefficient, r (as defined in [7]) is shown over the frequency range of simulation below in Figure 4-2. The allowable reflection coefficient range is shaded in the plot below. CST's PML boundary satisfies the specification throughout the benchmark frequency range.

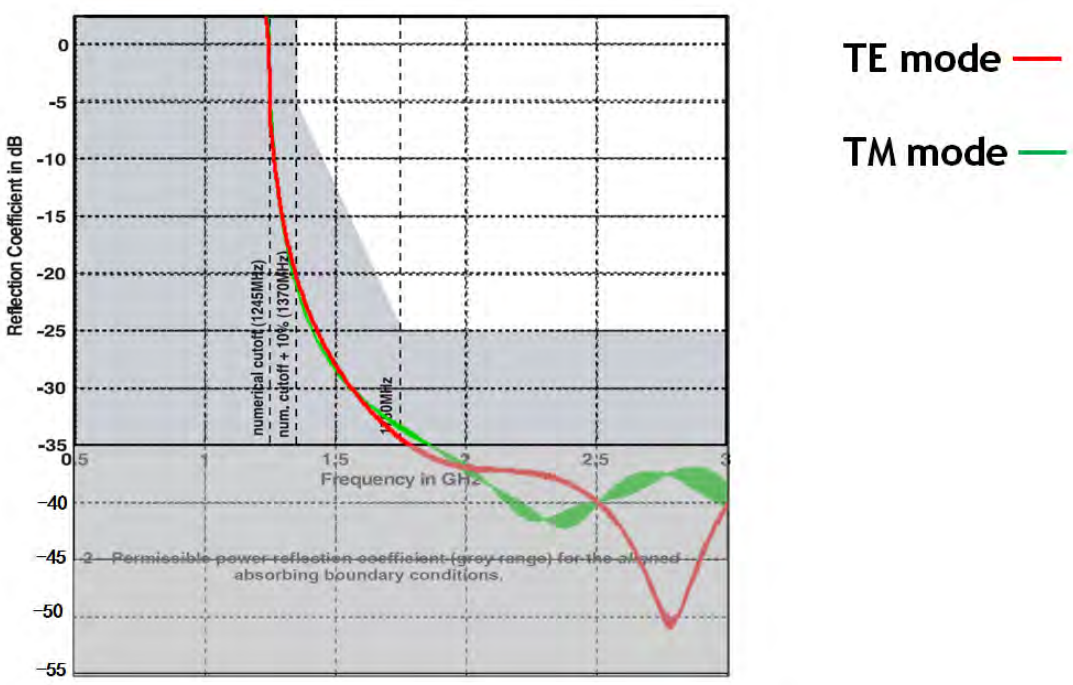

Figure 4-2: Reflection Coefficient for PML Boundary Test

Appendix 5 Dipole SAR Benchmark

As a validation case for SAR results obtained using the Finite Integration Technique, the system validation dipole and flat phantom contained with [14] was simulated, and the results were compared with the published SAR values at 900 and 3000 MHz as stipulated in [7].

The geometry of the dipole antenna and flat phantom tissue block were created according to the guidelines specified in the System Validation section of [14] and are listed below in Table 5-1

Frequency (MHz)	Dipole Length (mm)	Dipole Diameter (mm)	Dipole distance to phantom (mm)	Phantom Tissue Block (mm)	Shell Thickness (mm)
900	149	3.6	15	360 x 300 x 150	2
3000	41.5	3.6	10	220 x 160 x 150	2

Table 5-1: Dipole Benchmark Data

The dipole geometry utilized lossless metal material type. The material parameters for the phantom body and shell are shown below in Table 5-2.

Material	Relative Permittivity	Conductivity (S/m)	Mass Density (kg/m^3)
Body	38.5	2.4	1000
Shell	3.7	-	-

Table 5-2: Material parameters

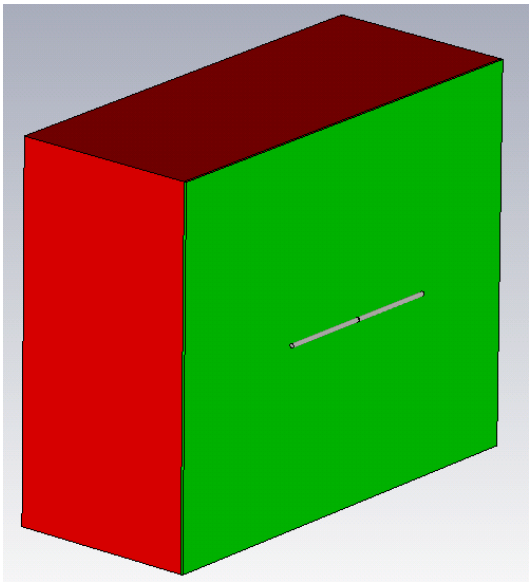

Figure 5-1: Dipole and Flat Phantom Geometry

Simulation settings used were consistent with those employed for the full device. A maximum cell size of 1/20 of a wavelength in a given material at the maximum frequency was utilized. A maximum frequency 1.5 times larger than the operating frequency was used in each case. This resulted in maximum cell sizes of 11.5727 mm and 3.47083 for 900 and 3000 MHz respectively. The dipole curvature was refined on a local level using a step size of one quarter the diameter.

The simulation volume was terminated in a perfectly matched layer (PML) absorbing boundary, spaced ¼ of the operating frequency wavelength away from the model geometry.

The steady state operation of the dipole was approximated by terminating the simulation when the energy contained within the simulation volume decayed to a level 60 dB below the peak value.

The resulting 1g and 10g SAR results were computed and are listed below in Table 5-3, along with the reference values from [1528-2003] and their relative percentage error.

Frequency (MHz)	**Simulated 1 g SAR (W/kg)**	**Reference 1 g SAR (W/kg)**	**Error (%)**	**Simulated 10 g SAR**	**Reference 10 g SAR (W/kg)**	**Error (%)**
900	10.128	10.8	6.222	6.822	6.9	1.130
3000	66.653	63.8	4.471	26.278	25.7	2.249

Table 5-3: 1 and 10 g Simulated SAR values

Additionally, the instantaneous point SAR value was computed at a point directly adjacent to the feed point on the surface of the phantom, as well as at a point 2 cm transversal from the feed, in accordance with the procedure outlined in [14]. Results are presented below in Table 5-4.

Simulated Local SAR at Phantom Surface (W/kg)	Reference Local SAR at Phantom Surface (W/kg)	Error (%)	Simulated Local SAR at surface (2 cm offset) (W/kg)	Reference Local SAR at surface (2 cm offset) (W/kg)	Error (%)
15.800	16.4	3.659	5.254	5.400	2.704
155.025	140.2	10.574	9.283	9.5	2.284

Table 5-4: Point SAR Values

For both sets of results, the error margin is several orders of magnitude less than the range by which the device operates under the SAR limits.

Appendix 6 SAR Bowl Benchmark

Due to the fact that measurements in true biological human heads typically cannot be conducted, SAR norms for mobile phones or EMI problems are commonly defined in terms of standardized phantom models. In the easiest case only spherical structures are considered. To predict the SAR behavior of a new product already during the design stage, it is desirable to include the phantom head in the EM simulations.

The following examples investigate two spherical phantom models, a basic one that only contains of tissue material inside a glass sphere and a more complex one that has two additional layers of bone and tissue. A dipole antenna is used for the excitation and is displayed as a yellow line in figure 6-1.

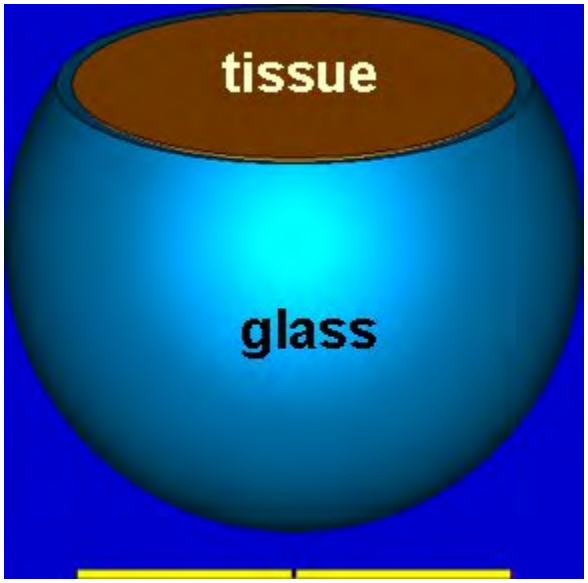

Figure 6-1: Basic spherical phantom head containing tissue material in glass. The yellow lines represent the exciting dipole antenna.

The SAR distribution is simulated at 835 MHz and visualized in the figure below. A comparison of the SAR values over a radial line shows good agreement with the measurement of the same structure.

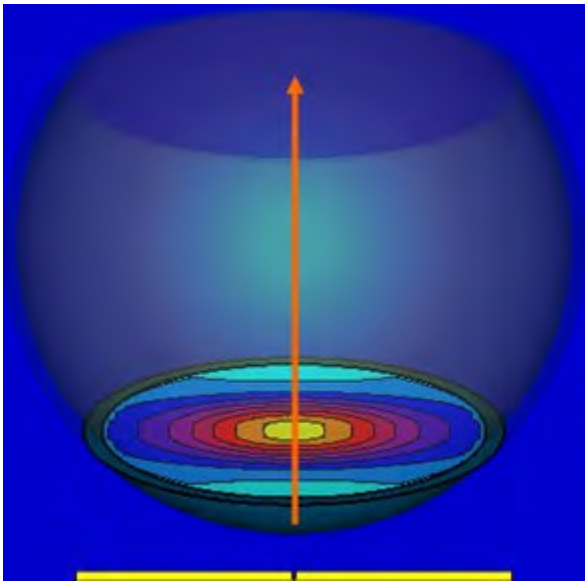

Figure 6-2: SAR values in a 2D plane inside the phantom model.

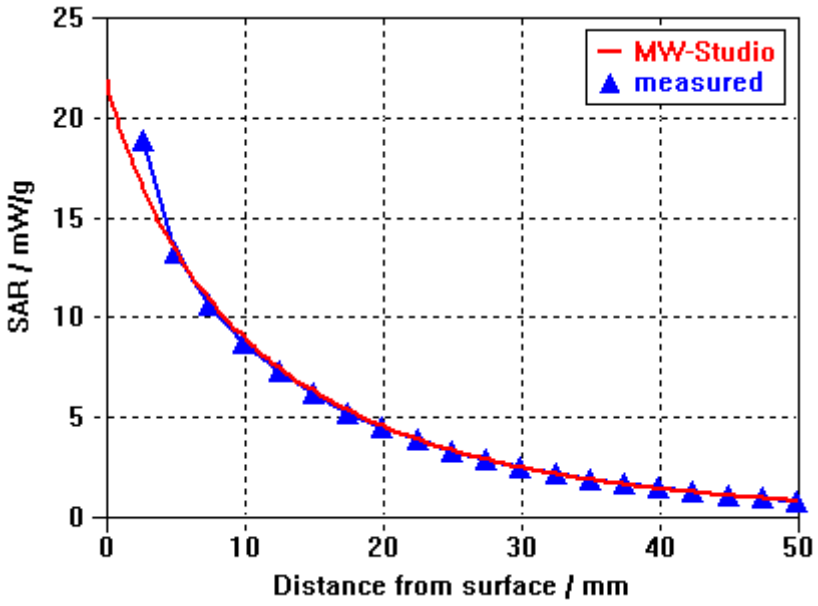

Figure 6-3: Comparison of simulation and measurement results along the orange arrow in the previous figure.

For the following simulation a more complex model including a simplified skull is used.

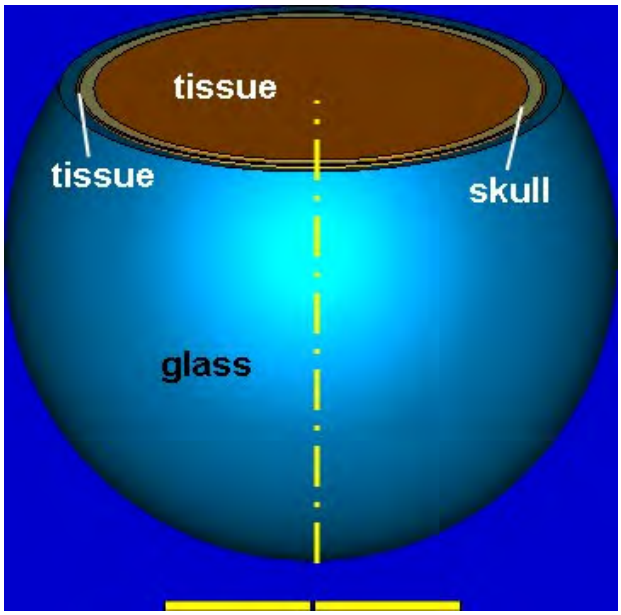

Figure 6-4: Inhomogeneous phantom model including a simplified skull.

A comparison of the SAR values at 1.95 GHz on an off-axis path shows a significant difference between the basic homogeneous model and the more complex one. Since the values are higher the simplified model may not be sufficient in all cases.

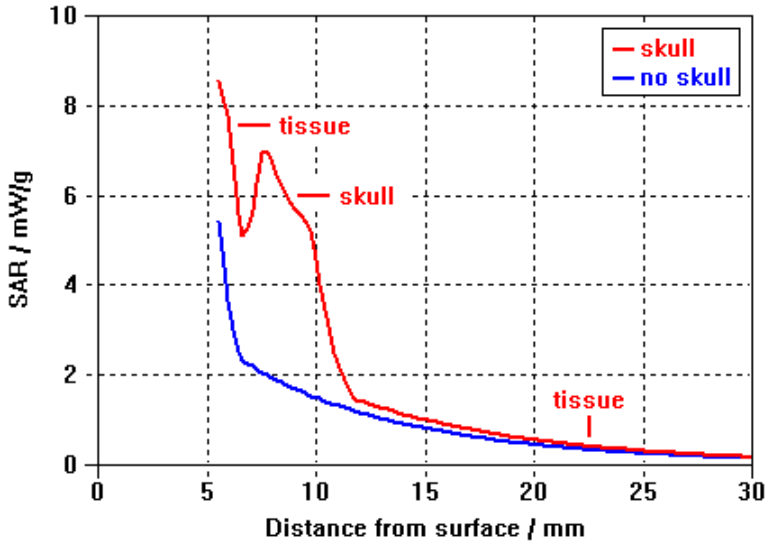

Figure 6-5: Comparison of the SAR values at 1.95 GHz for the basic and the inhomogeneous model.